Journal of Computational Physics **161,** 114–139 (2000)
doi:10.1006/jcph.2000.6492, available online at http://www.idealibrary.com on IDEAL®

High-Order Fluxes for Conservative Skew-Symmetric-like Schemes in Structured Meshes: Application to Compressible Flows

F. Ducros,* F. Laporte,* T. Soulères,* V. Guinot,† P. Moinat,* and B. Caruelle*

**Centre Européen de Recherche et de Formation Avancée en Calcul Scientifique, CERFACS, 42, Avenue Gaspard Coriolis, 31057 Toulouse Cedex, France; †International Institute for Infrastructure Hydraulics and Environmental Engineering, IHE, P.O. Box 3015, 2601 DA Delft, The Netherlands*
E-mail: ducros@cerfacs.fr

Received June 22, 1999; revised November 30, 1999

Developing high-order non-dissipative schemes is an important research task for both steady and unsteady flow computations. We take as a starting point the "built-in" de-aliasing property of the discretized skew-symmetric form for the non-linear terms of the Navier–Stokes equations, recalled in Kravchenko and Moin [1]. Two families of high-order locally conservative schemes matching this discretized skew-symmetric form are considered and rewritten in terms of telescopic fluxes for both finite difference and finite volume approximations in the context of compressible flows. The Jameson's scheme [2] is shown to be the second-order member of larger families of "skew-symmetric-like" centered schemes. The fourth-order finite volume and finite difference and the sixth-order finite difference schemes which belong to this family are provided. The proposed schemes are extended to shock capturing schemes, either by modifying the Jameson's artificial viscosity or by hybriding the centered flux with Weno [3] fluxes. An adapted interpolation is proposed to extend the use of the proposed schemes to non-regular grids. Several tests are provided, showing that the conjectured order is properly recovered, even with irregular meshes and that the shock capturing properties allow us to improve the second-order results for standard test cases. The improvement due to fourth-order is then confirmed for the estimation of the growth of two- (TS waves) and three- (Crow instability) dimensional unstable modes for both confined and free-shear flows. The last application concerns the steady computation using the Spalart–Allmaras model of a separated boundary layer: it confirms that the use of a high-order scheme improves the results, even in this type of steady applications.

Key Words: finite difference scheme; finite volume scheme; compressible flow; aliasing errors; high-order schemes.

0021-9991/00 $35.00

1. INTRODUCTION

Simulations of unsteady compressible flows are rapidly developing for applications such as acoustics, multi-physics flow, and in a generic way, LES/VLES (large-eddy simulations, very large-eddy simulations). These studies are no longer reserved to the research community but start a breakthrough in industrial-type applications. An important part of these studies concerns the development of high-order numerical schemes. For example, Shur *et al.* make use of a fourth-order centered and a fifth-order upwind scheme to perform detached eddy simulations [4] for both isotropic turbulence as well as for flows around an airfoil at high lift angle.

Although some LES are performed using second-order numerical schemes [5, 6], the general idea is that LES require higher-order schemes, especially for the convective part of the Navier–Stokes equations. The numerical errors can be considered as the sum of truncation and aliasing errors as presented in Lilly [7] and in Kravchenko and Moin [1]. This means that the notion of order is not sufficient to characterize a numerical scheme: one has also to consider properties such as conservation, dispersion, diffusion, or dissipation of directly transported quantities and of their possible quadratic invariants (kinetic energy, for example).

• *The description of the convective terms.* For compressible applications, weakly dissipative schemes are often used, even for LES applications. Indeed, one has to face two difficulties, which makes the built-in diffusion of some schemes attractive. First, most codes devoted to compressible applications are written using collocated variables. This prevents the users from benefitting from the stabilizing properties of staggered meshes. Second, compressible applications such as internal aerodynamics sometimes generate spurious acoustic waves, that may be damped by any built-in numerical diffusion.

However, as many modeling procedures are based on the Boussinesq approximation, i.e., on the use of an eddy viscosity ((V)-LES, U-RaNS, RaNS except second-order modeling), the use of weakly dissipative schemes is seen as a requirement to reduce spurious numerics/modeling interactions. This renders the use of centered schemes still attractive, because they do not exhibit any spurious diffusion or dissipation (when considered independently of the temporal scheme used to integrate the equation).

A far as the convective part of the compressible Navier–Stokes equations is concerned, the mentioned properties of conservation, dispersion, and dissipation strongly depend on the nature of the scheme (centered or upwind-biased) and on the form used for the discretization of the non-linear terms. This can be illustrated by considering the non-linear one-dimensional scalar equation

$$\frac{\partial U}{\partial t} + H = \frac{\partial U}{\partial t} + \frac{\partial UV}{\partial x} = \frac{\partial U}{\partial t} + \frac{\partial F(U)}{\partial x} = 0. \tag{1}$$

Although the divergence

$$H_{div} = \frac{\partial UV}{\partial x}, \tag{2}$$

convective

$$H_{conv} = U\frac{\partial V}{\partial x} + V\frac{\partial U}{\partial x}, \tag{3}$$

and skew-symmetric forms

$$H_{skew} = \frac{1}{2}\left(\frac{\partial UV}{\partial x}\right) + \frac{1}{2}\left(U\frac{\partial V}{\partial x} + V\frac{\partial U}{\partial x}\right) \tag{4}$$

are equivalent at the continuous level, these discretized forms do not have the same properties of conservation and stability. It is commonly admitted that kinetic energy conservation is a key feature for the stability of unsteady computations. This property is ensured in the incompressible limit by the skew-symmetric form (Eq. (4)) for centered schemes (see [1, 8], among many).

Conservation of quadratic quantities (such as kinetic energy) is presented as a resulting property of aliasing errors minimization in [7, 1]: Fourier analysis of forms (1) to (4) shows that it is the skew-symmetric form that minimizes aliasing errors. Conservation and de-aliasing properties of schemes have been extensively studied in the mid-1960s by the geophysical community and proper solutions have been proposed: the former work of Arakawa [9] has been extended by Lilly [7] to the primitive equations of motion, including eventually compressibility (see [7, Eq. 2.10]). Lilly derived a systematic way to get the quadratic-conserving representation of the transported quantities up to second order. As mentioned by a referee, the use of a skew-symmetric form for compressible flow is introduced in Feiereisen *et al.* [10].

• *Local conservation and finite volume formulation.* A property of importance for the numerical scheme is local conservation of transported quantities, which is the numerical translation of the conservation laws over a fixed finite volume Ω of fluid, and reads, for the previous one-dimensional equation,

$$\frac{\partial \int_\Omega U d\Omega}{\partial t} + \int_{S(\Omega)} \mathbf{F}\cdot\mathbf{d}S = 0, \tag{5}$$

where $\mathbf{F}$ is the flux at the surface $S(\Omega)$, oriented with the unit normal vector $\mathbf{d}S$. Let us consider the cell i, located at position x_i, of interfaces located at $x_{i+1/2}$ and $x_{i-1/2}$ (see Fig. 1). For Eq. (1), the discretized counterpart of Eq. (5) is written

$$\frac{\partial \int_\Omega U d\Omega}{\partial t} + F_{i+1/2}S_{i+1/2} - F_{i-1/2}S_{i-1/2} = 0, \tag{6}$$

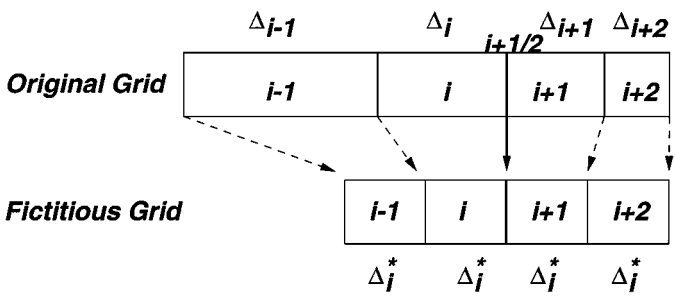

FIG. 1. Principle of interpolation for finite volume scheme on an irregular one-dimensional grid. An optimal fictitious regular grid is defined. The corresponding cells dimension is denoted by Δ_i^*. The interface $i+1/2$ where the flux is evaluated remains at the same location.

$F_{i+1/2}S_{i+1/2}$ being the flux through the interface located at $i+1/2$ ($F=UV$). Equation (6) ensures that any flux $F_{i+1/2}S_{i+1/2}$ leaving the cell i goes into cell $i+1$. This obviously ensures exact conservation of U and is known as the telescopic property introduced by Lax and Wendroff [11]. This property is of first importance for finite volume formulation and for compressible problems.

As shown by Eq. (4), typical skew-symmetric schemes are not written in a locally conservative form, which is not an issue in a finite difference (FD) context for incompressible flows but can be more questionable when used for compressible applications and is incompatible with the finite volume (FV) formulation. Recently, Morinishi *et al.* [8, 12] derived conservative second- and fourth-order schemes for LES of incompressible flows, including non-uniform grid arrangement studies. A recent solution to get high-order conservative skew-symmetric schemes was also derived by Veldman and Verstappen [13] for staggered meshes: this work emphasizes the conservative properties of the skew-symmetric form and proposes an original way to take varying meshes into account. However, its application to full Navier–Stokes equations requires the definition of two control volumes, one being three times larger than the standard control volume [14]. So, the issue of locally conservative schemes matching the skew-symmetric form and compatible with Eq. (6) is still an open question.

• *The search for finite volume/finite difference conservative schemes with skew-symmetric properties for compressible flows.* The present work is motivated by the search for high-order non-dissipative but numerically stable conservative schemes to perform unsteady calculations of compressible flows oriented towards LES and/or VLES. It is mainly inspired by

• the interest of the built-in de-aliasing property of the skew-symmetric form of centered schemes,

• the necessity of developing an implicit time marching method for unsteady calculations in complex geometry, which leads in practice to consider separate time and space integration.

This leads us to consider the following points:

• Whatever the interest of conservation of some quadratic quantities (such as kinetic energy) that comes along with the use of the skew-symmetric form of the convective term in the context of incompressible flow (see [1]), the use of such schemes for compressible flows is, for us, first motivated by the benefit obtained from the built-in de-aliasing property mentioned before. For the compressible equations considered here, kinetic energy is in balance with acoustic energy and we will not develop any discussion concerning its conservation: the interested reader is asked to refer to the existing literature. For the following, the conservative properties of the scheme will refer to the conservation of transported quantities, which will be guaranteed by the use of the flux-based formulation (Eq. (6)).

• The skew-symmetric form has already been used in conjunction with many different methods: spectral schemes [15], Padé schemes [16, 17], and more basically centered difference schemes (the last reference in that context is [12]). However, the use of such a form in a finite volume context, i.e., in a formulation based on Eq. (6), has, to the author's knowledge, never been exposed. The determination of such fluxes is the key issue of the paper. In order to be complete, the text will provide fluxes that when used will bring standard divergence

or skew symmetric forms (see the precise definition below) for both finite difference and finite volume contexts.

This limitation of the work will have the following consequences:

- Because we solve compressible Navier–Stokes equations, the conservative variables are chosen and the pressure P is explicitly solved. So, contrary to what has been done in [12] and other work, we do not take special care for the continuity equation $\partial\rho/\partial t + \partial\rho u_i/\partial x_i = 0$; the resolution is performed using the proposed fluxes, either in divergence or in skew-symmetric form.
- We will not follow the same discrimination between the divergence and the skew-symmetric forms as Morinishi *et al.* [12]. We will call the divergence (respectively skew-symmetric) form of order *n* any discretization of Eq. (1) that will match the discretization of Eq. (2) (resp. Eq. (4)) *using the nth order central differencing scheme.* This classification lays emphasis on the aliasing error reduction coming from the skew-symmetric form (see [6, 18]). Moreover, our definition asserts the fact that the skew-symmetric and the divergence forms match in the compressible context at a discretized level only if the convection equation is a linear one. The direct consequence is that the relations provided in Morinishi *et al.* [12] are incompatible with the present definition.

As introduced in [19], the starting point of the proposed family of fluxes is the original scheme developed by Jameson *et al.* [2] and the fact that it is equivalent to a second-order skew-symmetric scheme (see below and [6, 18]).

We propose high-order (second, fourth, and sixth) centered skew-symmetric FD schemes and high-order (second, fourth) centered skew-symmetric-like FV schemes. All these schemes are developed for collocated variables and match the telescopic conservative property of Eq. (6). As they are centered, they do not present any diffusion for the transported quantities, at least for one-dimensional problems and non-diffusive time integration.

The paper is organized as follows. First, the formulations of the fluxes involved in FD or FV discretization of the Euler equations are recalled (Subsection 2.1). To concentrate on conservation properties, both FD and FV discretizations are rewritten as flux divergences (Eq. (6)). The second-order Jameson scheme (SOJS) is then presented, including the formulation of the fourth- and second-order artificial dissipations (Subsection 2.2). The constraints on the searched schemes (centered, skew-symmetric-like, controlled order) are formulated in a mathematical way, which leads to a linear system, for which the SOJS is the only solution corresponding to the second-order scheme (Section 3). The particular solutions concerning the fourth-order are then proposed (Section 3). An extension of the schemes to varying meshes (Section 5) and an adaptation of the centered flux to shock-capturing schemes using either modified second-order artificial viscosity or hybridazation with a fifth-order Weno scheme (Section 4) are finally proposed. The schemes are implemented in an industrial solver (Section 6). The results concerning one-, two-, and three-dimensional test cases are then proposed and prove the good behavior of the numerical method (Sections 7 and 8). The complete Taylor expansion showing the order of the schemes is provided in an appendix, together with the sixth-order scheme of the proposed family. All schemes presented here are derived for structured data. In the following, the conservative property that is verified by the presented schemes concerns the transported quantities. The conservation of the kinetic energy is ensured through the skew-symmetric form in the incompressible limit (see [1]).

2. CONSERVATIVE SCHEMES

2.1. Generalities on conservative schemes. For all following developments, variables are collocated and cell-centered: they stand alternatively for the local (for FD, $U_{i,j,k} = U(x_{i,j,k})$) or for the mean value of U over the cell (for FV, $\hat{U}_{i,j,k} = \frac{1}{\mathcal{V}} \int_{\mathcal{V}(\mathbf{x}_{i,j,k})} U(\mathbf{x})\, \mathbf{dx}$, $\mathcal{V}(\mathbf{x}_{i,j,k})$ is the volume of the cell located at $\mathbf{x}_{i,j,k}$ in the physical space and designed by the coordinates i, j, k in a structured code). Let $\mathcal{S}_{i+1/2,j,k}$ be the surface of the interface between cells i, j, k and $i+1, j, k$. Let us consider the local Euler equations, involving the fluxes F^n in the nth direction,

$$\frac{\partial W}{\partial t} + \operatorname{div}(F^n) = 0, \tag{7}$$

with

$$W = (\rho, \rho u^1, \rho u^2, \rho u^3, \rho e)^T, \qquad F^n(W) = \begin{pmatrix} \rho u^n \\ \rho u^n u^1 + p\delta_{n1} \\ \rho u^n u^2 + p\delta_{n2} \\ \rho u^n u^3 + p\delta_{n3} \\ u^n(\rho e + p) \end{pmatrix}, \qquad \operatorname{div}(F^n) = \sum_{n=1}^{3} \frac{\partial F^n}{\partial x_n}. \tag{8}$$

u^n is the local velocity in the nth direction. For simplicity, only semi-discrete schemes and one-dimensional conservation equations will be considered. We restrict our search to locally conservative schemes. Such schemes can therefore be written in a form that matches the Lax and Wendroff telescopic property. Then, the discretization of Eq. (8) in the direction i using either a cell-centered FD or FV technique can be expressed as

$$\frac{\partial W_i}{\partial t} + \frac{F^{FD}_{i+1/2} - F^{FD}_{i-1/2}}{\Delta_i} - \mathcal{E}^{FD}_i = 0, \tag{9}$$

$$\mathcal{V}_i \frac{\partial \hat{W}_i}{\partial t} + F^{FV}_{i+1/2}\mathcal{S}_{i+1/2} - F^{FV}_{i-1/2}\mathcal{S}_{i-1/2} - \mathcal{E}^{FV}_i = 0. \tag{10}$$

$\mathcal{E}^{FV}_i$ and $\mathcal{E}^{FD}_i$ stand for the truncation error of the method. $F^{FD}_{i+1/2}$ and $F^{FV}_{i+1/2}$ are the numerical fluxes at the interface between cells i and $i+1$. As far as FD and FV approaches are concerned, one may distinguish between:

- High-order FD schemes, where a high-order approximation of the derivative $(\frac{\partial F}{\partial x})_i$ at point i is looked for. The evaluation of the order directly comes from the Taylor expansion of the considered derivatives at point i involved in the local form of Eq. (7).
- High-order FV schemes, where a high-order approximation of the flux F at the interface is looked for. The evaluation of the order directly comes from the Taylor expansion of the flux at the considered interface $i+1/2$. As detailed below, only the direction splitting method for FV will be considered here (cf. Section 3). A real multi-dimensional FV scheme will not be built here. However, the improvement due to an "high-order directionally split FV scheme" will be shown for many applications.

Formally, Eqs. (9) and (10) reduce to the same form when the mesh is regular: $\mathcal{V}_i = \mathcal{V}$, $\mathcal{S}_{i-1/2} = \mathcal{S}_{i+1/2} = \mathcal{S}$, and $\mathcal{V}/\mathcal{S} = \Delta$, except that FD formulations deal with local values

of the fields U_i, whereas FV formulations deal with averaged values $\hat{U}_i$. Finding proper expressions of the fluxes $F^{FD}_{i+1/2}(W)$ and $F^{FV}_{i+1/2}(\hat{W})$ is the motivation of the present paper.

2.2. Second-order Jameson scheme (SOJS). For the SOJS and for both FV and FD contexts (see below, Eq. (17)), the numerical flux $F_{i+1/2}$ is approximated by

$$F_{i+1/2} = F\left(W_{i+1/2}\right) - d_{i+1/2}, \tag{11}$$

where $d_{i+1/2}$ is a combination of second- and fourth-order artificial dissipation [2], with

$$d_{i+1/2} = d^{o2}_{o2,i+1/2} + d^{o4}_{o2,i+1/2}, \tag{12}$$

$$d^{o2}_{o2,i+1/2} = \epsilon^{(2)}_{i+1/2}(W_{i+1} - W_i), \tag{13}$$

$$d^{o4}_{o2,i+1/2} = -\epsilon^{(4)}_{i+1/2}(W_{i+2} - 3W_{i+1} + 3W_i - W_{i-1}), \tag{14}$$

and

$$\epsilon^{(2)}_{i+1/2} = k^{(2)}\mathcal{R}_{i+1/2}\Psi_{i+1/2}, \tag{15}$$

$$\epsilon^{(4)}_{i+1/2} = \max\left(0.0, k^{(4)}\mathcal{R}_{i+1/2} - \epsilon^{(2)}_{i+1/2}\right). \tag{16}$$

$k^{(2)}$ and $k^{(4)}$ are real numbers fixing the amount of diffusion brought up by the second- and fourth-order dissipative operators d^{o2}_{o2} and d^{o4}_{o2} (the superscripts $o2$ or $o4$ are related to the order of the diffusion operator used for the dissipation; the subscript $o2$ is related to the order of the scheme on which it applies). $\mathcal{R}_{i+1/2}$ is the spectral radius of the jacobian matrix $\partial F/\partial W$ at the cell face $i + 1/2$. The aim of the fourth-order artificial dissipation is to control (by preventing them) spurious oscillations. When the second-order artificial dissipation is switched on, the global scheme is close to an hybridization between centered and upwind schemes and is able to capture the shocks; $\Psi_{i+1/2}$ is a sensor based on pressure fluctuations (see Jameson [2, 20, 21]).

A Taylor expansion of W_i in the cell centered around i shows that

$$\hat{W}_i - W_i = \frac{\Delta^2}{24}\left(\frac{\partial^2 W}{\partial x^2}\right)_i. \tag{17}$$

This explains that the confusion between the FD and FV approximations can be made up to second order. We now expose two possible formulations for F in Eq. (11), one of them constituting the original Jameson scheme (see below).

2.3. A family of centered schemes. Up to Section 4, $k^{(4)}$, $k^{(2)}$ of Eqs. (15) and (16) are set to zero. The role played by the non-linearities and their different formulations (Eqs. (2)–(4)) in the complete compressible Navier–Stokes equations can be studied first on the one-dimensional scalar Eq. (1).

At first sight, all forms (Eqs. (2)–(4)) are meaningful in the FD context, but only the divergence form (Eq. (2)) can be used in the FV context. However, it is easy to identify in the existing literature the fluxes $F_{i+1/2}$ that, when plugged into the discrete divergence conservative form 9 or 10, will lead either to the second-order discretized divergence form (Eq. (2)) or to the second-order discretized skew-symmetric form (Eq. (4)).

Let us consider the developed expression of the second-order discretized divergence form

$$\frac{\partial U_i}{\partial t} + \frac{U_{i+1}V_{i+1} - U_{i-1}V_{i-1}}{2\Delta x} = \mathcal{E}^{div}_{o2,i} \tag{18}$$

and of the second-order discretized skew-symmetric form

$$\frac{\partial U_i}{\partial t} + \frac{1}{2}\left(\frac{U_{i+1}V_{i+1} - U_{i-1}V_{i-1}}{2\Delta x}\right) + \frac{1}{2}U_i\left(\frac{V_{i+1} - V_{i-1}}{2\Delta x}\right) + \frac{1}{2}V_i\left(\frac{U_{i+1} - U_{i-1}}{2\Delta x}\right) = \mathcal{E}^{skew}_{o2,i}. \tag{19}$$

It is easy to show that Eq. (18) is obtained when plugging

$$F_{i+1/2} = (U_i V_i + U_{i+1}V_{i+1})/2 = F^{div}_{o2,i+1/2} \tag{20}$$

in Eq. (9) or (10); whereas Eq. (19) is obtained when plugging

$$F_{i+1/2} = F(U_{i+1/2}) = \frac{(U_i + U_{i+1})}{2}\frac{(V_i + V_{i+1})}{2} = F^{skew}_{o2,i+1/2} \tag{21}$$

in Eq. (9) or (10) (see previous studies [6, 18, 19]). Please notice that the fluxes are written together with the mention of the discretization they produce (skew or div in superscript); the order is made precise by the subscript ($o2$ here). Equation (19) corresponds to the scheme given by Eq. (66) of Morinishi *et al.* [12]; it also corresponds to the SOJS.

Replacing U by $\hat{U}$ in Eqs. (18)–(21) leads to the same formal developments (see the Appendix). In conclusion, the Jameson scheme is a second-order conservative FD scheme in skew-symmetric form, or a second-order conservative FV scheme, where the flux divergence (as defined in Eq. (10)) is formally as close as possible to the standard skew-symmetric discretization (and is therefore denoted by "skew-symmetric-like"). For the present developments and since Eq. (17) holds, the corresponding FV form is identical to the FD one; there is no need to specify the FV or FD context here and the differences between the two schemes stands only at the concept level. This is no longer the case for higher-order schemes.

3. HIGH-ORDER EXTENSION ON REGULAR GRIDS

We now investigate the possibilities of constructing similar fluxes for nth-order centered schemes (n being an even number). For this, we introduce the more general non-linear flux that can lead to such schemes, first in the FD context (k, p are integers),

$$F^{FD}_{on,i+1/2} = \sum_{k,p\in\{i-n/2+1,i+n/2\}} \beta_{k,p} U_{i+p} V_{i+k}. \tag{22}$$

The $\beta_{k,p}$ are scalars depending only on the order of the scheme and on the local metrics. Notice that this procedure is similar to the one used by Lilly [7].

With $k = p$, we will seek for divergence schemes, whereas skew-symmetric schemes should be found with two different indices. In a very similar manner we write the $\mathcal{O}(n)$ approximation of the derivative of the scalar U at cell i as

$$\left(\frac{\partial U}{\partial x}\right)_i = \frac{1}{\Delta}\sum_{l\in\{i-n/2,i+n/2\}} \gamma_l U_{i+l}. \tag{23}$$

γ_l is directly obtained using standard Taylor expansions. In order to get consistent schemes, the coefficients should obey the following constraints: $\sum_l \gamma_l = 0$ and $\sum_{k,p} \beta_{k,p} = 1$. Centered schemes are obtained for $\gamma_l = \gamma_{-l}$, $\gamma_0 = 0$. The schemes we are looking for are determined by the $\beta_{k,p}$, solutions of

$$H_{div} = \sum_{l\in\{i-n/2,i+n/2\}} \gamma_l \frac{U_{i+l}V_{i+l}}{\Delta} = \sum_{k\in\{i-n/2+1,i+n/2\}} \beta_{k,k} \frac{(U_{i+k}V_{i+k} - U_{i-1+k}V_{i-1+k})}{\Delta} \quad (24)$$

for a scheme in divergence form (search for $F^{div,FD}_{on,i+1/2}$) and of

$$\begin{aligned} H_{skew} &= \frac{1}{2} \sum_{l\in\{i-n/2,i+n/2\}} \frac{(\gamma_l U_{i+l}V_{i+l} + U_i(\gamma_l V_{i+l}) + V_i(\gamma_l U_{i+1}))}{\Delta} \\ &= \sum_{k,p\in\{i-n/2+1,i+n/2\}} \beta_{k,p} \frac{(U_{i+p}V_{i+k} - U_{i-1+p}V_{i-1+k})}{\Delta} \end{aligned} \quad (25)$$

for a scheme in skew-symmetric form (search for $F^{skew,FD}_{on,i+1/2}$). For a given order n, the solution of Eq. (24) is unique; whereas Eq. (25) leads to a over-determined system of linear equations. The general solution of Eq. (25) for an arbitrary order n was not looked for. We provide hereafter a solution for $n = 4$; a solution for $n = 6$ is proposed in the Appendix.

The problem in the FV context is formulated nearly in the same manner. We introduce the flux

$$F^{VF}_{on,i+1/2} = \sum_{k,p\in\{i-n/2+1,i+n/2\}} \beta'_{k,p} \hat{U}_{i+p}\hat{V}_{i+k} \quad (26)$$

and, as suggested in the previous section, we look for the FV scheme, which presents the flux divergence as close as possible to the FD skew-symmetric or divergence form of same order: the corresponding fluxes will be superscripted *skew, FV* or *div, FV* in the following.

Let us consider regular grids in this section. For sake of clarity, the proofs concerning the order of the different schemes are reported in the Appendix.

3.1. Divergence form. It corresponds to $k = p$ and leads to

$$F^{div,FD}_{o4,i+1/2} = \frac{1}{12}(-U_{i+2}V_{i+2} + 7U_{i+1}V_{i+1} + 7U_iV_i - U_{i-1}V_{i-1}), \quad (27)$$

$$\begin{aligned} F^{div,FV}_{o4,i+1/2} &= \frac{1}{12}(-\hat{U}_{i+2}\hat{V}_{i+2} + 7\hat{U}_{i+1}\hat{V}_{i+1} + 7\hat{U}_i\hat{V}_i - \hat{U}_{i-1}\hat{V}_{i-1}) \\ &\quad + \frac{1}{3}\left(\frac{1}{2}(\hat{U}_{i+1}\hat{V}_{i+1} + \hat{U}_i\hat{V}_i) - \frac{1}{4}(\hat{U}_{i+1} + \hat{U}_i)(\hat{V}_{i+1} + \hat{V}_i)\right), \end{aligned} \quad (28)$$

which provides conservative centered fourth-order schemes for the FD and FV contexts, respectively. We recall that the cancellation of aliasing errors directly comes from the skew-symmetric form and holds for all similar expressions, whether this expression involves local (FD context) or averaged (FV context) values. There is thus no built-in de-aliasing in fluxes 27 and 28. That is why we look for skew-symmetric and "skew-symmetric-like" forms.

3.2. Skew-symmetric and skew-symmetric-like forms. In the FV context, a real high-order scheme ($n > 2$) is difficult to derive for a multi-dimensional context, just because the estimation of the flux at an interface as derived for the one-dimensional case is not enough. One should take into account the variation of the flux along the interface in other directions than the direction normal to the interface. Some solutions based on real multi-dimensional schemes have been proposed that lead to very expensive schemes. Under these circumstances, it appears to us that deriving a fourth-order FV scheme in a one-dimensional manner can be of interest, because of its analogy with the FD context described before.

A solution of Eq. (25) is

$$F^{skew,FD}_{o4,i+1/2} = \frac{1}{3}(U_i + U_{i+1})(V_i + V_{i+1}) - \frac{1}{24}(U_{i-1}V_{i-1} + U_{i-1}V_{i+1} + U_iV_i + U_iV_{i+2} + U_{i+1}V_{i+1} + U_{i+1}V_{i-1} + U_{i+2}V_i + U_{i+2}V_{i+2}). \tag{29}$$

The finite volume counterpart expression reads

$$F^{skew,FV}_{o4,i+1/2} = \frac{1}{3}(\hat{U}_i + \hat{U}_{i+1})(\hat{V}_i + \hat{V}_{i+1}) - \frac{1}{24}(\hat{U}_{i-1}\hat{V}_{i-1} + \hat{U}_{i-1}\hat{V}_{i+1} + \hat{U}_i\hat{V}_i + \hat{U}_i\hat{V}_{i+2} + \hat{U}_{i+1}\hat{V}_{i+1} + \hat{U}_{i+1}\hat{V}_{i-1} + \hat{U}_{i+2}\hat{V}_i + \hat{U}_{i+2}\hat{V}_{i+2}) + \frac{1}{3}\left(\frac{1}{2}(\hat{U}_{i+1}\hat{V}_{i+1} + \hat{U}_i\hat{V}_i) - \frac{1}{4}(\hat{U}_{i+1} + \hat{U}_i)(\hat{V}_{i+1} + \hat{V}_i)\right). \tag{30}$$

Equations (29) and (30) provide the fourth-order schemes for the FD and FV context, respectively. The flux 30 can be seen as the closer counterpart in the FV context of the skew-symmetric FD scheme provided by Eq. (29). Notice that Eq. (29), together with Eq. (9), corresponds to Eq. (72) of Morinishi *et al.*

Remark 1. Applying standard (non-compact) centered derivatives in the FD approximation of the skew-symmetric form Eq. (4) defines the same scheme as the one given by Eqs. (9) and (29) (Eq. (72) of Morinishi *et al.*). So, despite its formulation involving a non-conservative term such as $U_i\partial V_i/\partial x + V_i\partial U_i/\partial x$, the resulting scheme is conservative and matches the telescopic property.

4. SHOCK CAPTURING SCHEMES

Some applications involving strong discontinuities may also require the use of a low-level dissipative scheme in other parts of the flow. This is the case for turbulent flow developing together with interface corrugations (Rayleigh–Taylor and Richtmyer–Meshkov instabilities, shock-turbulence interaction). This is also the case for stationary and unsteady aerodynamics applications (flow around an aircraft in transonic cruise conditions, for example).

For both situations the use of the previous scheme may be suggested, provided some procedure to cope with discontinuities may be found. We hereafter present two ways to construct such a scheme:

- The first one consists of the use of artificial viscosity, as done for the SOJS (see Eqs. (11)–(16), together with $k^{(2)} > 0$). To understand how this dissipation works, the one-dimensional linear scalar equation

$$\frac{\partial U}{\partial t} + a\frac{\partial U}{\partial x} = 0, \qquad a > 0 \tag{31}$$

is often considered [22]. The use of the SOJS applied to this equation leads to a second-order centered scheme, except in the region where the second-order dissipation d_{o2}^{o2} acts. Assuming that the expression $\epsilon^{(2)}$ (see Eq. (13)) takes locally the value $a/2$, then the flux globally reads

$$F(U_{i+1/2}) - d_{o2,i+1/2}^{o2} = aU_i, \tag{32}$$

$$F_{i+1/2} - F_{i-1/2} - \left(d_{o2,i+1/2}^{o2} - d_{o2,i-1/2}^{o2}\right) = a(U_i - U_{i-1}). \tag{33}$$

The scheme is locally switched from centered second order to upwind first order. This property (the "upwind connection" in Swanson and Turkel [22]) is advocated to explain the "good" behavior of the Jameson scheme applied to equivalent non-linear systems [6]. Let us call d_{o4}^{o2} the artificial viscosity that would be added to the fourth-order flux to get an upwind like scheme. The first choice is of course

$$d_{o4}^{o2} = d_{o2}^{o2}, \tag{34}$$

for which the global flux $F_{o4,i+1/2} - d_{o4,i+1/2}^{o2}$ is not able to switch to a true upwind scheme, whatever the value $\epsilon^{(2)}$. A better adapted artificial viscosity d_{o4}^{o2} can be built so that the expression $F_{o4,i+1/2} - d_{o4,i+1/2}^{o2}$ may recover the same upwind scheme as in Eq. (33) for $\epsilon^{(2)} = a/2$:

$$d_{o4,i+1/2}^{o2} = \frac{2\epsilon_{i+1/2}^{(2)}}{12}(-U_{i+2} + 7U_{i+1} - 5U_i - U_{i-1}). \tag{35}$$

Notice that, as the main objective of this artificial viscosity is to make the scheme switch from a central to first-order upwind scheme, no special care is required to distinguish between FD or FV schemes here.

- The other solution consists in an hybridization between the centered scheme and an upwind one in regions where discontinuities occur. The corresponding flux reads as

$$F_{i+1/2} = \Phi_{i+1/2} F_{o4,i+1/2} + \left(1 - \Phi_{i+1/2}\right) F_{upwind}. \tag{36}$$

In order to preserve high-order, F_{upwind} may be the flux given by a fifth-order Weno scheme [3]: this gives the C4W5-hybridization scheme. The *w*eighted *e*ssentially *n*on-*o*scillatory (Weno) scheme consists of building a high-order ENO reconstruction procedure together with a Riemann solver (Roe solver in practice here). Φ is a sensor that detects the steep gradient regions; $\Phi = \Psi$ is the first choice [6]. In this context and as the Weno formulation relies on high-order schemes, a special care concerning the context of FD or FV should be taken to build a consistent scheme.

These two methods are to be used in different conditions. The second one is of course more accurate and is recommended for unsteady simulations, although it is more expensive. However, the former, even if it is cruder, is cheaper and allows better convergence properties for steady simulations. Indeed, such a hybridization can make the scheme switch from one form to another one for some cells, preventing the corresponding local residual from going to zero, even with an efficient Newton method.

5. NON-UNIFORM GRID SYSTEM

The global order of a given method goes down for any varying meshes if the mesh variations are not taken into account. Recent works [13] propose to account for the metrics in a "weak way," preferring to conserve stability properties of the scheme for the "*global* discretization," rather than ensuring a constant and known "*local* discretization error": this leads to a reduced order (up to first-order) but stable scheme (see Veldman and co-workers [13, 23]). As pointed out in Morinishi *et al.* [12], one must make a choice between strict conservation and maintaining accuracy.

In a first attempt, we try to stick to standard approaches and to maintain the local order of the scheme when using varying meshes. As clearly exposed below, this will lead to fourth-order schemes, able to ensure the local conservation of the transported quantities but unable to ensure kinetic energy conservation, which is consistent with the global approach developed here. The main difficulty in extending the present scheme to non-uniform grids relies on the fact that non-local products arise in the formulations of the fluxes. The problem formulated in Eqs. (24) and (25) and in their counterparts for the FV context can be reformulated in order to take into account the mesh variation (γ_l and $\beta_{k,p}$ are functions of the node positions x_i, x_{i+1}, etc.). However, if we can find a solution for the divergence form, no solution can be found for the skew-symmetric form. A direct derivation of the metric based on a standard Taylor expansion is thus not possible. It is the reason why we only retain the two following ways to take the metrics into account.

5.1. Finite difference context. A practical way to deal with the non-uniform grid is to consider a derivable mapping between the real grid (x, y, z) and a regular mapping $(\xi(x, y, z), \eta(x, y, z), \phi(x, y, z))$. Then, the standard method relies on the development based on Jacobian matrices,

$$\frac{\partial F}{\partial x} = \frac{\partial F}{\partial \xi}\frac{\partial \xi}{\partial x} + \frac{\partial F}{\partial \eta}\frac{\partial \eta}{\partial x} + \frac{\partial F}{\partial \phi}\frac{\partial \phi}{\partial x}, \tag{37}$$

which ensures the global order of the derivatives to be conserved, provided the order of all derivations is homogeneous. In practice it is recommended to use the same scheme for all derivatives [13, 24]. But we did not manage to find any conservative approximation of Eq. (37).

Remark 2. The "conservativity" of the scheme can be maintained for a flux of the form $F_{FD,i+1/2}\mathcal{G}_{i+1/2}$, $\mathcal{G}_{i+1/2}$ being an estimation of $(\frac{\partial \xi}{\partial x})_i$. However, such an estimation is possible only up to first order, which makes the global order of the scheme decrease. The property of conservativity of the standard skew-symmetric schemes derived using centered derivatives discussed in Remark 1 is thus limited to the regular grid.

5.2. Finite volume context. We now present the generalization of this scheme in an irregular Cartesian context. The method presented here directly applies to any FV centered scheme and was inspired by Shu [3]. Of course for 2 or 3 dimensions, the global order of the scheme will fall to second order, for the reason coming from Eq. (17). We recall that from a practical point of view, FV schemes based on one-dimensional stencils provide obvious improvements compared to lower-order schemes.

Because we have a high-order scheme on regular meshes, the idea simply lies in the possibility to use this scheme on a fictitious regular grid. We present here a method to

realize this idea in a simple way. At each interface $i+\frac{1}{2}$, we associate a fictitious regular grid, whose spacing Δ_i^* is chosen to be the optimal spacing (according to a certain criterion made precise below) over the stencil used for the calculation of the flux. Since we will use an interpolation polynomial, the fictitious grid is proposed to be the largest that can be used. As shown in Fig. 1, the grid spacing Δ_i^* is then defined by

$$2\Delta_i^* = \min(\Delta_{i-1} + \Delta_i, \Delta_{i+1} + \Delta_{i+2}). \tag{38}$$

We focus on high-order approximation of the flux at the interface $i+\frac{1}{2}$. Given the mean values $\hat{U}_j$, $J \in \{i-1, i, i+1, i+2\}$ on the irregular mesh, we can obtain high-order approximation of the mean values $\hat{U}_j^*$, $J \in \{i-1, i, i+1, i+2\}$ on the optimal fictitious grid. The method to recover these mean values is as follows: we first define the primitive of U over the considered stencil

$$V(x) = \int_{x_{i-2+\frac{1}{2}}}^{x} U(\xi)\, d\xi.$$

The knowledge of the mean values on the irregular grid is equivalent to the knowledge of the primitive at interfaces since

$$\begin{aligned} V\left(x_{j+\frac{1}{2}}\right) &= \int_{x_{i-2+\frac{1}{2}}}^{x_{j+\frac{1}{2}}} U(\xi)\, d\xi \\ &= \sum_{k=i-2}^{j} \hat{U}_k \Delta_k, \quad j \in \{i-2, i-1, i, i+1, i+2\}. \end{aligned}$$

We now define the Lagrange polynomial $P(x)$ which interpolates the primitive V at the locations of the interfaces,

$$P(x) = \sum_{j=i-2}^{i+2} V\left(x_{j+\frac{1}{2}}\right) \prod_{k=1-2, k\neq j}^{i+2} \frac{x - x_{j+\frac{1}{2}}}{x_{k+\frac{1}{2}} - x_{j+\frac{1}{2}}}.$$

This polynomial provides the following approximation in case of a regular mesh,

$$P(x) = V(x) + \mathcal{O}(\Delta^5) \qquad \forall x \in \left[x_{i-2+\frac{1}{2}}, x_{i+2+\frac{1}{2}}\right].$$

In case of an irregular mesh, the order of approximation is linked to the derivative of order 5 of V, and to the distribution of the grid points. Nevertheless, we assume that for reasonable grid stretching rates, this approximation remains suitable, and we denote $\Delta = \max((\Delta_j)_{j\in\{i-1,i,i+1,i+2\}})$. The coordinates of the fictitious grid are defined such that the interface $i+\frac{1}{2}$ under concern has not moved,

$$x^*_{i+k+\frac{1}{2}} = x_{i+\frac{1}{2}} + k\Delta_i^*, \qquad k \in \{-2, -1, 0, 1, 2\}.$$

The pointwise values of P at these locations yield

$$P\left(x^*_{i+k+\frac{1}{2}}\right) = \int_{x_{i-2+\frac{1}{2}}}^{x^*_{i+k+\frac{1}{2}}} U(\xi)\, d\xi + \mathcal{O}(\Delta^5).$$

Consequently the fictitious mean values can be approximated at high order in the following

way,

$$\hat{U}_j^* = \frac{1}{\Delta_i^*}\left[P\left(x^*_{j+\frac{1}{2}}\right) - P\left(x^*_{j-1+\frac{1}{2}}\right)\right] + \mathcal{O}(\Delta^4), \qquad j \in \{i-1, i+2\}.$$

Note that the subscript of Δ_i^* is i, no more depending on the location j since the fictitious grid is regular. The order of approximation finally obtained (4) is consistent with the order of the proposed scheme (4). The complete formula is

$$\hat{U}_j^* \simeq \frac{1}{\Delta_i^*} \sum_{j=i-2}^{i+2} \sum_{k=i-2}^{j} \hat{U}_k \Delta_k \left[\prod_{k=i-2, k\neq j}^{i+2} \frac{x^*_{j+\frac{1}{2}} - x_{j+\frac{1}{2}}}{x_{k+\frac{1}{2}} - x_{j+\frac{1}{2}}} \prod_{k=i-2, k\neq j}^{i+2} \frac{x^*_{j-1+\frac{1}{2}} - x_{j+\frac{1}{2}}}{x_{k+\frac{1}{2}} - x_{j+\frac{1}{2}}} \right]$$

which explicitly gives the fictitious mean values from the real mean values and the local metric of the mesh. Once this reconstruction is done, the original numerical FV flux can be simply applied to the reconstructed mean values in order to evaluate the flux at interface $i + 1/2$.

As stressed before, the resulting schemes conserve the transported quantities, and the use of the proposed interpolation has two consequences:

- First, it can act as a smoothing that could be able to dissipate kinetic energy. One may draw some parallel between the present interpolation and the standard parabolic interpolation appearing in the piecewise parabolic method (see Collela and Woodward [25]).
- Second, it interferes with the strictly skew-symmetric form, and therefore results in an increase of aliasing errors.

6. IMPLEMENTATION

The previous schemes are now called SOJS for the second-order Jameson scheme, COSSYL-FV4 (respectively, -FD4) for the fourth-order conservative skew-symmetric FV (respectively FD) like schemes. All have been implemented in a vectorial/parallel version of the FV structured multi-block solver NSMB developed in an academic/industrial type consortium gathering Aérospatiale, Saab, CERFACS, KTH, and EPFL [26]. This code solves the complete compressible Navier–Stokes Eqs. (7) and (8), together with LES and RaNS modelings. Independent implementation and tests of the sixth-order scheme in a "research code" prove that it performs well, even better than the fourth-order scheme for the Cartesian grid. However, if the existing NSMB architecture is well adapted to the stencils involved in the fourth-order schemes, it is not the case for the larger stencils involved in the sixth order, which is no longer considered in the present paper.

As stressed by the rewriting of the FD scheme in a conservative manner (see Eq. (9)), one can easily switch from a FV to a FD code for Cartesian meshes, which allows the testing of both types of approaches. As far as time integration is concerned, standard Runge–Kutta explicit as well as implicit time integrations can be used, since the proposed schemes rely on separate time and space discretizations. For explicit Runge–Kutta schemes, the stability condition adapted for the present schemes is not different from the stability condition arising for standard centered schemes; the interested reader can find all the details in [27]. For implicit integration, no stability condition arises and we make use of the scheme already available in the solver, namely, a Newton method based on *l*ower-*u*pper-symmetric *G*auss–*S*eidel (LU-SGS) schemes for steady flows, developed by Weber [18, 28].

TABLE I
Estimation of the CPU Cost of Several Schemes Used for Compressible Application, Normalized by the Cost of the SOJS

Scheme	SOJS	COSSYL-FV4 No Met.	Weno-Roe
CPU cost	1	1.2	5
Scheme	C4W5-hybridization	COSSYL-FV4 Fu. Met.	Weno-Roe Fu. Met.
CPU cost	$1.2 \leq \cdot \leq 5$	4	15

Note. The present cost concerns the time spent to evaluate the Euler part of Navier–Stokes equations; No Met. stands for no metric; Fu. Met. for full metric. The cost of the C4W5-hybridization scheme strongly depends on the test case and on the way to implement the two fluxes.

Table I provides an estimation of the CPU cost of several schemes used for compressible applications, normalized by the cost of the SOJS. The present cost concerns the time spent to evaluate the spatial derivatives (building of the fluxes and divergence estimation) and concerns only direction splitting schemes: no true multi-dimensional scheme is considered here. Relating directly the results of the following test cases to the properties of the proposed schemes can be done as follows. The advantage of using an high-order scheme will clearly appear in the examples. However, the aliasing reduction due to the use of the skew-symmetric form appears at small scales (see Kravchenko and Moin [1]). This means that the use of the divergence form in most of the presented cases where the skew-symmetric form performs well will end in a blow-up of the code. This is due to spurious oscillations in the thermodynamic fields: most of this unfavorable behaviour is related with wiggle developments. In consequence, no simulation will be presented using the divergence form.

7. LAMINAR ONE- AND TWO-DIMENSIONAL TEST CASES

The global order of each scheme is proved in the Appendix using formal mathematical developments. We hereafter provide numerical tests, showing the good behaviour of the proposed schemes.

7.1. One-dimensional test case. The aim of this section is to compare numerical with reference solutions in some particularly simple configurations such as acoustic waves or one-dimensional shocks. For this, we consider the evolution of the cumulative error as a function of $\Delta(n)$

$$\epsilon(n) = \sum_{i=1}^{n} \left\| \rho_i - \rho_i^{th} \right\|, \tag{39}$$

where ρ_i^{th} is the analytical solution of the problem at the considered time and n is the number of points used for discretization of a domain of fixed length L_x; $\Delta(n) = L_x/(n-1)$.

• *Acoustic wave.* We first consider the case of a Gaussian acoustic wave $\rho(x) = \rho_0 + \delta\rho e^{-(1/\sigma^2)(x-L_x/2)^2}$ that propagates in a periodic domain of length $L_x = 1$ for the Euler equations, $\sigma = 0.03$, and $\delta\rho = 0.01$. The use of similar test cases to investigate dispersive and diffusive properties of schemes is usual; see [29], for example. Obviously, the order of the scheme is recovered on a regular grid. Moreover, in order to check the order of the proposed COSSYL-FD4 metric and COSSYL-FV4 metric schemes, two fixed stretchings (5 and 15%) are investigated. The resolution varies between 200 and 1600 points. For each

mesh, the domain is discretized in five zones: (1) zone 1, the step size dx_1 is constant; (2) zone 2, the step size is locally refined with a fixed stretching over 20 points, dx_i thus varies from dx_1 to dx_2; (3) zone 3, the constant step size dx_2 is taken over $L_x/2$; (4) zone 4, the step size then increases from dx_2 to dx_1; (5) zone 5, the step size is constant and equal to dx_1. This allows us to test the effect of mesh stretching on the solution, the ratio between the smaller and the larger cells being kept constant. Figure 2 provides $\epsilon(n)$ for the SOJS and the COSSYL-FD4 and COSSYL-FV4 schemes after one convection time (the wave is back on its initial location). Despite the stretching and thanks to the skew-symmetric formulation, the presents results are obtained without artificial damping ($k^{(4)} = k^{(2)} = 0$). The results obtained with the fourth-order schemes are always better than the one obtained using the second-order scheme. Only the consideration of the metric can ensure the expected order, which is quite intuitive.

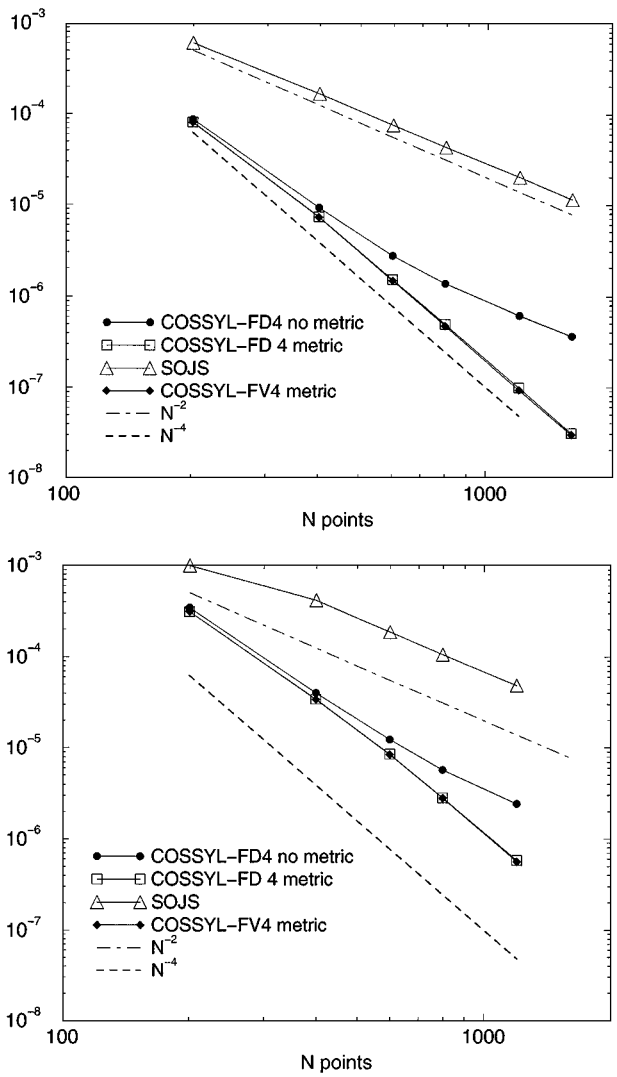

FIG. 2. Error between the analytical and calculated solutions for an acoustic wave, for 5% (top) and 15% (bottom) stretching. "No metric" means that the fourth-order scheme is used without metric. $k^{(2)} = k^{(4)} = 0$.

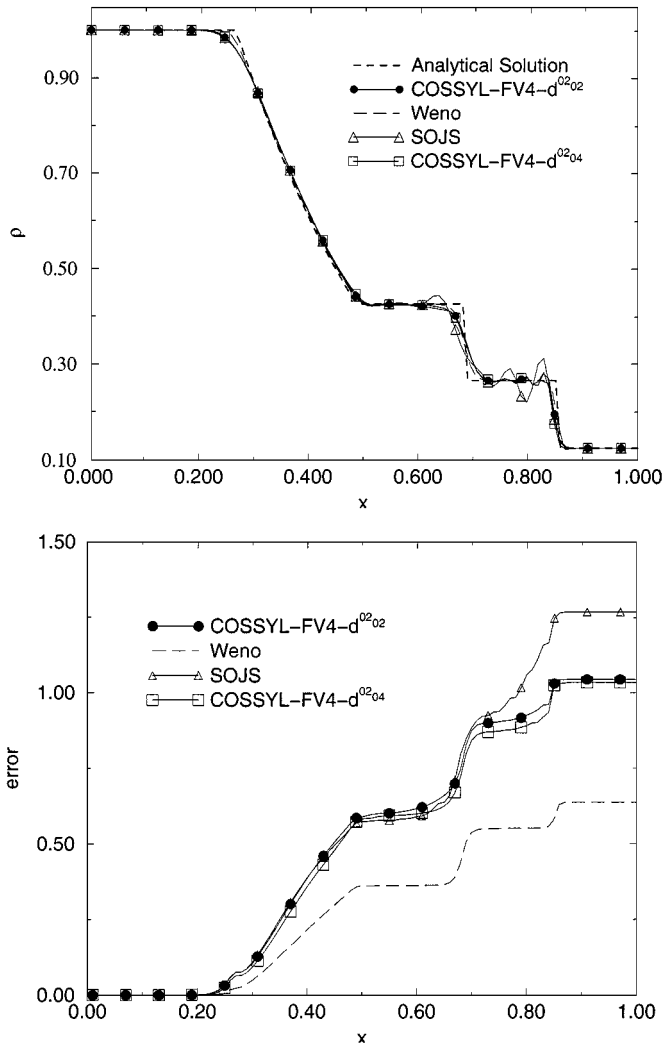

FIG. 3. Top, comparison between analytical solution and results from simulations using Weno, second-, and fourth-order schemes for the Sod test case at $t = 0.2Lx/U_{ref}$. Bottom, cumulative errors for simulations of the Sod test case.

• *Sod test case.* The description of this very common test case can be found in [30]. The top of Fig. 3 gives a comparison between the analytical solution and results (at $t = 0.2Lx/U_{ref}$) from simulations using Weno (fifth order), SOJS, and COSSYL-FD4 using both d_{o2}^{o2} (Eq. (34)) and d_{o4}^{o2} (Eq. (35)) artificial dampings. Here, we tune the artificial viscosity with $k^{(2)} = 0.5$ and $k^{(4)} = 0.03$ for both second- and fourth-order schemes. The better results are of course obtained with the Weno scheme. The results given by the C4W5-hybridization and using Weno only are the same for the chosen sensor Φ, but strongly depend on this choice (results not shown here). When comparing SOJS and COSSYL-FV4, the use of the fourth-order scheme allows a better treatment of the expansion wave and reduces the oscillations near the shock and the contact discontinuity. This fact is more pronounced when using the adapted artificial damping d_{o4}^{o2} rather than the original d_{o2}^{o2}, which produces surprisingly good results. All these properties are recovered in Fig. 3 where we plot $\epsilon(n)$.

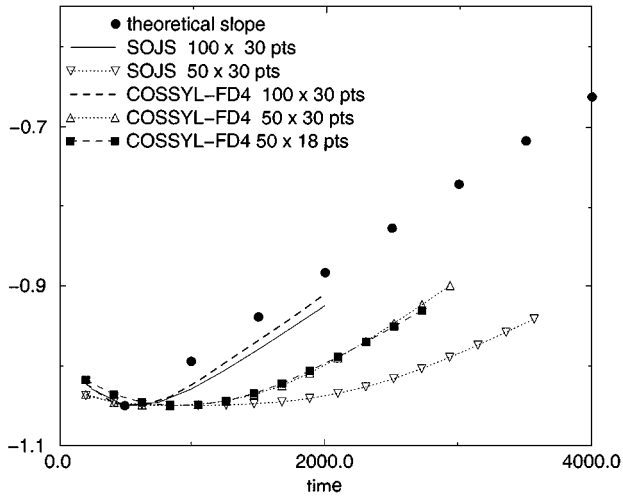

FIG. 4. Amplification rate of the Tollmien–Schlichting wave.

7.2. Two-dimensional unsteady test case: Tollmien–Schlichting waves. Concerning unsteady flows, the use of high-order non-diffusive numerical schemes is particularly interesting in the frame of instability development. Bayliss *et al.* [31] compute the growth rate of waves in spatially developing subsonic and supersonic boundary layers over a flat plate; they compared second- and fourth-order Mac Cormack schemes.

We hereafter compute the growth rate of temporally developing Tollmien–Schlichting waves for a weakly compressible boundary layer (free stream Mach number 0.5) for a Reynolds number based on the displacement thickness δ_i of $Re_{\delta_i} = 1000$. The initial condition consists of the 2D laminar compressible boundary layer together with an incompressible white nosie of weak amplitude (10^{-4}): the dimensions of the domain are $(22, 20)\delta_i$. The configuration is supposed to be periodic, which means that the flow leaving the domain is reinjected at the inlet. The laminar growth of the layer thickness is treated through a classical forcing described in [32]. Based on linear, compressible stability theory it is known that the length $22\delta_i$ corresponds to an unstable wavelength of Tollmien–Schlichting waves (see Schlichting [33] for incompressible flow, and Mack [34] for compressible boundary layers). The expected growth rate is $\omega_i \approx 1.82 U_\infty/\delta_i$ for our case and has been reported in Fig. 4. This figure shows the growth rate of TS waves for several resolutions. Here, the viscous terms of the Navier–Stokes equations are evaluated through the standard second-order centered scheme already implemented in the NSMB solver. The COSSYL-FD4 scheme allows us to follow the development of such waves even for resolutions where the SOJS is not able to ensure the wave amplification. For all simulations, $k^{(2)} = k^{(4)} = 0$.

8. THREE-DIMENSIONAL TEST CASES

In a former study, it was shown that the use of the proposed fourth-order rather than second-order schemes improves the results for LES computations of attached turbulent boundary layers, at least as turbulent fluctuations are concerned [19], as it is usually reported [1]. Two test cases are provided hereafter; the first concerns the development of Crow instability and is close to DNS ($k^{(2)} = k^{(4)} = 0$); the second is close to aerodynamics and includes RaNS modeling.

8.1. Simulation of the long-wavelength Crow instability developing in vortex pairs. This test case is performed using explicit time stepping in a pure Euler context. It aims at evaluating the gain obtained with the COSSYL-FV4 scheme with respect to the SOJS scheme in a typical configuration dominated by convection phenomena. The long-wavelength three-dimensional instability developing in originally two-dimensional rectilinear vortex pairs has been discovered by Crow [35] and is of major concern in the field of wake vortex. The dynamics of this instability has been further investigated theoretically by Widnall *et al.* [36]. The physical mechanism is due to the velocity induced by one vortex on the other, and also to the self-induced velocity of one vortex. The most amplified wavelength scales with the vortex separation distance (denoted by b). This wavelength, as well as the associated growth rate, depends on the ratio a/b, where a stands for the vortex core radius. In the present test case, we use a superposition of two rectilinear Lamb–Oseen vortices without axial velocity, such as the initial ratio is $a/b \simeq 0.2$. Periodic boundary conditions are used in the three directions. The simulation domain is chosen to contain three wavelengths of the Crow instability in its axial dimension ($L_x = 18b$). Obviously this axial size of domain has some influence on the simulated most amplified wavelength if the size does not exactly match the natural wavelength. The transverse dimensions are defined such as the vortex replica induced by the periodic boundary conditions having a weak influence on the considered vortex pair. A good compromise is found to be $L_y = 5.5b$ and $L_z = 4.5b$. Three grid resolutions have been used (see Table II). The number of points in each dimension is denoted by n_x, n_y, and n_z. Time is put to the non-dimensional form ($t^* = t(u_{ref}/l_{ref})$). We only focus on the linear regime of the instability development. The simulation on the fine mesh with the COSSYL-FV4 is considered as the reference simulation (Fig. 5). The evolution of the mode corresponding to Crow instability is identified by performing axial discrete Fourier transforms. Figure 6 shows the evolution of the kinetic energy contained in the simulated mode corresponding to the instability mode. The reference solution shows that a transient period before the kinetic energy corresponding to the Crow mode is exponentially amplified. On the coarse mesh the SOJS provides a growth rate close to the reference up to a non-dimensional time $t^* \simeq 60$. This early departure from the reference curve indicates that the intrinsic dispersion of the scheme acts strongly on the vortices. Indeed some vortical patches are extracted from the initial vortices and the solution becomes non-physical. On the same coarse mesh, the fourth-order scheme eventually diverges from the reference curve later ($t^* \simeq 85$). The medium mesh allows much more pertinent comparisons with the reference solution. In this case both schemes show a good qualitative behaviour. The growth rate simulated by the SOJS is overpredicted after $t^* = 135$ and exhibits an increase in deviation, whereas the growth rate simulated by the COSSYL-FV4 corresponds to the reference curve up to $t^* = 150$, and the deviation observed remains approximately constant

TABLE II
Mesh Resolutions for Crow Instability Development

Mesh	n_x	n_y	n_z
Fine	115	92	40
Medium	80	60	30
Coarse	60	41	22

Note. nx, ny, nz describes the resolution in x, y, and z directions.

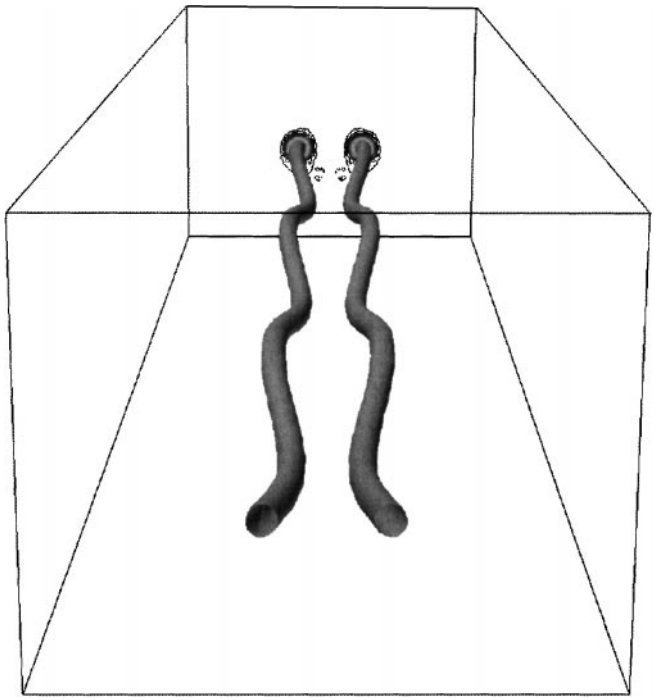

FIG. 5. Structure of the Crow instability at time $t^* = 250 L_{ref}/U_{ref}$. Fine mesh and COSSYL-FV4.

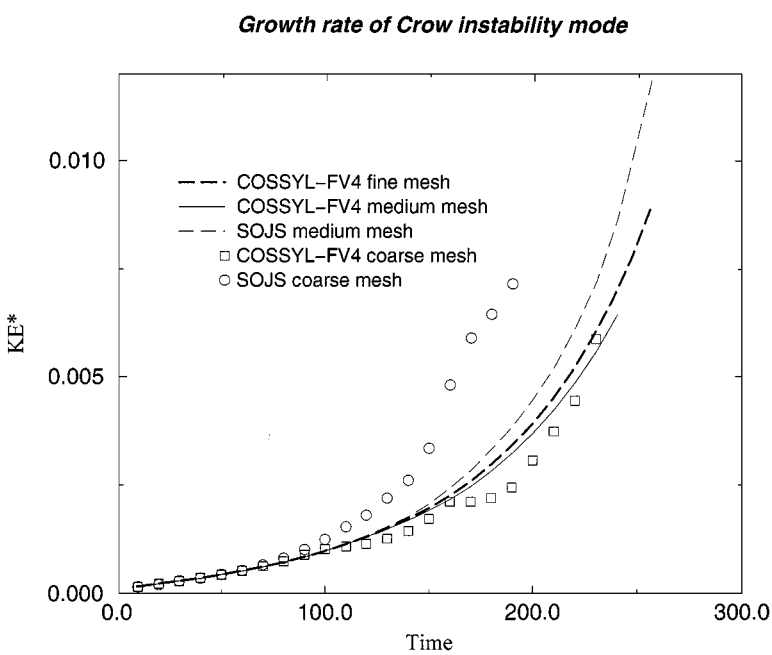

FIG. 6. Evolution of the kinetic energy in Crow mode development as function of time for different schemes and grid resolutions.

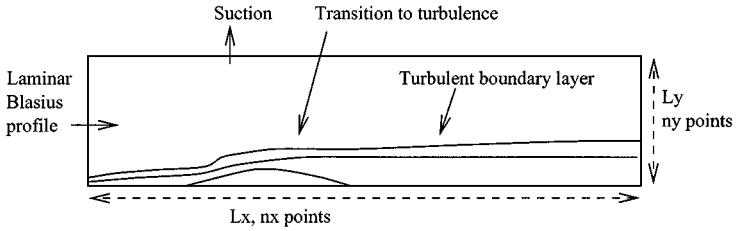

FIG. 7. Computational set up for the detached laminar boundary layer.

up to late stages. In conclusion, this test case provides a concrete proof of the improvement accomplished by the COSSYL-FV4 for the prediction of three-dimensional unsteady flows.

8.2. Steady RaNS computation. The pertinence of a high-order scheme for steady RaNS computations is still an open question. However, we compute the solution of the RaNS equations, solved together with the Spalart–Allmaras (S–A) model [37] on the configuration described in Fig. 7. This corresponds to the simulation of the transition to turbulence of a laminar boundary layer submitted to an adverse pressure gradient caused by a suction on the upper wall. The problem here is not to know if the solution is a good one, but to analyze how the scheme is able to converge towards a grid independent solution. The grid is stretched near the wall and the resolution is kept constant in the vertical direction for all simulations ($L_y = 100\delta_1$, δ_1 being the inlet displacement thickness, $ny = 100$). The grid is discretized using a regular step size in the streamwise direction ($L_x = 350\delta_1$, nx varies between 150 to 600). For all simulations, the transport equation of the S–A model is resolved using a first-order scheme, whereas the time evolution of the other conservative variables is computed using either the second- or the fourth-order scheme; the second-order artificial viscosity is set to zero, whereas the fourth-order artificial viscosity is set to a standard value for steady simulations $k^{(4)} = 1/64$. Figure 8 shows that a given mesh convergence is achieved using the most refined mesh for both second- and fourth-order schemes. This result is

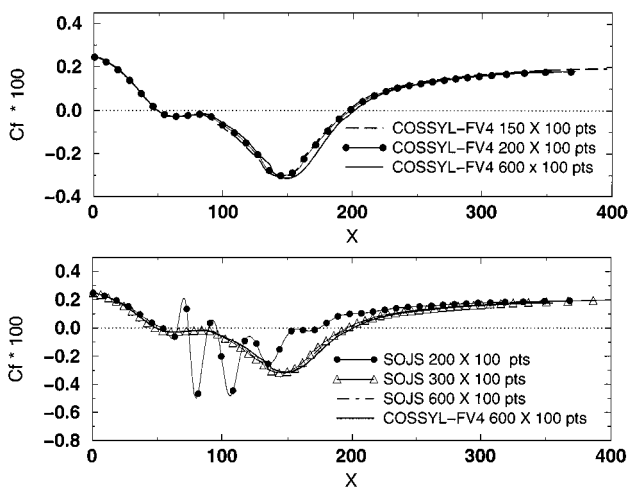

FIG. 8. Friction coefficient for steady RaNS simulation of separated boundary layer. Top, COSSYL-FV4 results, and bottom, SOJS results; for both figures, the result obtained on the (600×100) grid is taken as reference.

preserved for coarser resolution using the fourth-order scheme whereas the use of the second-order scheme is not able to reach a converged solution for medium resolution ($nx = 200$): the fourth-order scheme thus allows a large CPU cost reduction (approximately 50%, linked to the 2 time coarser grid), which is compared to the 20% CPU cost increase of the fourth- versus second-order fluxes computation.

9. CONCLUSION

From a theoretical point of view, we have integrated the second-order Jameson scheme in a larger family of schemes presenting skew-symmetric or "skew-symmetric-like" properties. The derivation of these schemes is proposed in three steps:

- First, the fluxes corresponding to a given order are found for a regular grid arrangement as the solution of an over-determined system of linear equations following some additional constraints (Section 3).
- Second, the extension for an irregular grid is proposed through the use of high-order Lagrange polynomials (Section 5).
- Eventually, specific artificial dissipation or hybridization with an high-order upwind flux is proposed (Section 4).

In conclusion, the FD (respectively FV) proposed fluxes lead to conservative, skew-symmetric (respectively skew-symmetric-like), fourth-order schemes. From a practical point of view, the previous schemes have been tested in an industrial code and have shown to behave well for various test cases, including steady and unsteady simulations (Sections 7 and 8). The expected order is checked and a systematic improvement is obtained when using the fourth-order instead of the second-order scheme. Additional tests (not reported here) have clearly confirmed the stabilizing property of the skew-symmetric form.

10. APPENDIX: THEORETICAL DETERMINATION OF THE ORDER

This section proposes formal developments of truncation errors of the considered schemes up to sixth order. All developments are performed using the formal solver Mathematica and are available on demand.

10.1. Finite volume vs finite difference approximations. We recall that

- for the FD context, finding a nth-order approximation of Eq. (1) consists of finding an approximation of the derivative H, such as

$$H = \frac{\partial UV}{\partial x} = \frac{\partial F^{true}}{\partial x} = \frac{\partial F^{num}}{\partial x} + \mathcal{O}\left(\Delta_x^n\right); \tag{40}$$

- for the FV context, $\hat{U}_i = (1/\mathcal{V}_i)\int_{\mathcal{V}_i} U(x, y, z)\, d\mathcal{V}_i$, and finding a high-order approximation of Eq. (1) then consists of finding a nth-order approximation of the fluxes at the interface $x_{i+1/2}$ such as

$$\begin{aligned}\frac{1}{\mathcal{V}_i}\int_{\mathcal{V}_i} H\, d\mathcal{V}_i &= \frac{1}{\mathcal{V}_i}\int_{\mathcal{V}_i} \frac{\partial UV}{\partial x}\, d\mathcal{V}_i = \frac{F^{true}_{i+1/2} - F^{true}_{i-1/2}}{\Delta_x} \\ &= \frac{F_{i+1/2} + \mathcal{O}\left(\Delta^{n+1}_{x_{i+1/2}}\right) - \left(F_{i-1/2} + \mathcal{O}\left(\Delta^{n+1}_{x_{i-1/2}}\right)\right)}{\Delta_x}.\end{aligned} \tag{41}$$

10.2. Finite difference approximation.

- *Second-order scheme.* The fluxes 20 and 21 define respectively

$$\frac{F_{o2_{i+1/2}}^{div,FD} - F_{o2_{i-1/2}}^{div,FD}}{\Delta} = \left[\frac{\partial uv}{\partial x}\right]_{x_i} + \left(\mathcal{O}_{o2}^{div,FD}\right)_{x_i}, \tag{42}$$

$$\frac{F_{o2_{i+1/2}}^{skew,FD} - F_{o2_{i-1/2}}^{skew,FD}}{\Delta} = \left[\frac{\partial uv}{\partial x}\right]_{x_i} + \left(\mathcal{O}_{o2}^{skew,FD}\right)_{x_i}. \tag{43}$$

Standard Taylor expansions of the continuous variable $U(x)$ and $V(x)$ around point x_i leads to

$$\left(\mathcal{O}_{o2}^{div,FD}\right)_{x_i} = \frac{\Delta_x^2}{2}(u'v'' + u''v')_{x_i} + \frac{\Delta_x^2}{6}\left(uv^{(3)} + vu^{(3)}\right)_{x_i} + \mathcal{O}\left(\Delta_x^4\right) \tag{44}$$

$$\left(\mathcal{O}_{o2}^{skew,FD}\right)_{x_i} = \frac{\Delta_x^2}{4}(u'v'' + u''v')_{x_i} + \frac{\Delta_x^2}{6}\left(uv^{(3)} + vu^{(3)}\right)_{x_i} + \mathcal{O}\left(\Delta_x^4\right). \tag{45}$$

The intuitive notation $u' = \partial u/\partial x$; $u'' = \partial^2 u/\partial x^2$ is adopted. The corresponding schemes are second order in space.

- *Fourth-order scheme.* For Eqs. (27) and (29), the Taylor expansion leads to

$$\left(\mathcal{O}_{o4}^{div,FD}\right)_{x_i} = \frac{\Delta_x^4}{30}\left[\frac{\partial^5 uv}{\partial x^5}\right]_{x_i} + \mathcal{O}\left(\Delta_x^6\right) \tag{46}$$

$$\begin{aligned}\left(\mathcal{O}_{o4}^{skew,FD}\right)_{x_i} = {} & \frac{\Delta_x^2}{6}\left[u^{(3)}v'' + u''v^{(3)}\right]_{x_i} + \frac{\Delta_x^4}{12}\left[u^{(4)}v' + u^{(4)}v'\right]_{x_i} \\ & + \frac{\Delta_x^4}{30}\left[uv^{(5)} + uv^{(5)}\right]_{x_i} + \mathcal{O}\left(\Delta_x^6\right).\end{aligned} \tag{47}$$

The corresponding schemes are fourth order in space.

- *Sixth-order scheme.* $\beta_{k,p}$ as defined by Eq. (22) can be found for higher-order schemes. The following flux

$$\begin{aligned}F_{o6,i+1/2}^{div,FD} = {} & \frac{1}{60}(U_{i+3}V_{i+3} - 8U_{i+2}V_{i+2} + 37U_{i+1}V_{i+1} \\ & + 37U_iV_i - 8U_{i-1}V_{i-1} + U_{i-2}V_{i-2})\end{aligned} \tag{48}$$

used in Eq. (9) leads to

$$\begin{aligned}\left(\mathcal{O}_{o6}^{div,FD}\right)_{x_i} = {} & \frac{\Delta_x^6}{140}\left(35v^{(3)}u^{(4)} + 35u^{(3)}v^{(4)} + 21v''u^{(5)} + 21u''v^{(5)} + 7v'u^{(6)}\right. \\ & \left. + 7u'v^{(6)} + vu^{(7)} + uv^{(7)}\right)_{x_i} + \mathcal{O}\left(\Delta_x^8\right).\end{aligned} \tag{49}$$

Concerning the skew-symmetric formulation, the flux

$$\begin{aligned}F_{o6,i+1/2}^{skew,FD} = {} & \frac{1}{120}(37U_iV_i + 45U_{i+1}V_i - 9U_{i+2}V_i + U_{i+3}V_i + U_{i-2}V_{i-2} + U_{i+1}V_{i-2} \\ & - 8U_{i-1}V_{i-1} - 9U_{i+1}V_{i-1} + U_{i+2}V_{i-1} + 45U_iV_{i+1} + U_{i-2}V_{i+1} - 9U_{i-1}V_{i+1} \\ & + 37U_{i+1}V_{i+1} - 9U_iV_{i+2} + U_{i-1}V_{i+2} - 8U_{i+2}V_{i+2} + U_iV_{i+3} + U_{i+3}V_{i+3})\end{aligned}$$

leads to

$$\left(\mathcal{O}_{o6}^{skew,FD}\right)_{x_i} = \frac{\Delta_x^6}{120}\left(15v^{(3)}u^{(4)} + 15u^{(3)}v^{(4)} + 9v''u^{(5)} + 9u''v^{(5)} + 3v'u^{(6)} + 3u'v^{(6)} + \frac{6vu^{(7)}}{7} + \frac{6uv^{(7)}}{7}\right)_{x_i} + \mathcal{O}\left(\Delta_x^8\right).$$

The corresponding scheme is sixth order in space.

10.3. Finite volume approximation.

- *Second-order scheme.* The fluxes

$$\begin{aligned} F_{o2,i+1/2}^{skew,FV} &= (\hat{U}_i + \hat{U}_{i+1})(\hat{V}_i + \hat{V}_{i+1})/4, \\ F_{o2,i+1/2}^{div,FV} &= (\hat{U}_i\hat{V}_i + \hat{U}_{i+1}\hat{V}_{i+1})/2 \end{aligned} \tag{50}$$

provide the following approximation of F at the interface

$$F_{o2,i+1/2}^{div,FV} = F_{i+1/2}^{true} + \Delta^2\left(\frac{u'v'}{4} + \frac{vu''}{6} + \frac{uv''}{6}\right)_{x_{i+1/2}} + \mathcal{O}\left(\Delta_x^4\right) \tag{51}$$

and

$$F_{o2,i+1/2}^{skew,FV} = F_{i+1/2}^{true} + \Delta^2\left(\frac{vu''}{6} + \frac{uv''}{6}\right)_{x_{i+1/2}} + \mathcal{O}\left(\Delta_x^4\right). \tag{52}$$

The fluxes thus propose a second-order approximation of the real flux at the interface, leading to a second-order scheme in a FV context.

- *Fourth-order scheme.* The previous high-order fluxes Eqs. (28) and (30) give

$$F_{o4,i+1/2}^{div,FV} = F_{i+1/2}^{true} - \Delta_x^4\left(\frac{7u''v''}{36} + \frac{v'u^{(3)}}{8} + \frac{u'v^{(3)}}{8} + \frac{vu^{(4)}}{30} + \frac{uv^{(4)}}{30}\right)_{x_{i+1/2}} + \mathcal{O}\left(\Delta_x^6\right) \tag{53}$$

and

$$F_{o4,i+1/2}^{skew,FV} = F_{i+1/2}^{true} - \Delta_x^4\left(\frac{u''v''}{9} + \frac{v'u^{(3)}}{24} + \frac{u'v^{(3)}}{24} + \frac{vu^{(4)}}{30} + \frac{uv^{(4)}}{30}\right)_{x_{i+1/2}} + \mathcal{O}\left(\Delta_x^6\right). \tag{54}$$

They propose a fourth-order approximation of the real flux at the interface, leading to a fourth-order scheme in a FV context.

- *Link between FV and FD.* With the previous explanations, the truncation error in the FV context reads

$$F_{on,i+1/2}^{FV} = F_{i+1/2}^{true} - \Delta^n\mathcal{F}_{i+1/2} + \mathcal{O}(\Delta^{n+2}) \tag{55}$$

with $\mathcal{F}_{i+1/2}$ a function of $[(\partial^p u/\partial x^p)/(\partial^q v/\partial x^q)]_{x_{i+1/2}}$ with $p+q=n$, which with Eq. (10) leads to

$$\frac{F_{i+1/2}^{true} - F_{i-1/2}^{true}}{\Delta} = \frac{F_{on,i+1/2}^{FV} - F_{on,i-1/2}^{FV}}{\Delta} + \Delta^n\frac{\mathcal{F}_{i+1/2} - \mathcal{F}_{i-1/2}}{\Delta}, \tag{56}$$

i.e.,

$$\frac{F^{true}_{i+1/2} - F^{true}_{i-1/2}}{\Delta} = \frac{F^{FV}_{on,i+1/2} - F^{FV}_{on,i-1/2}}{\Delta} + \Delta^n \left(\frac{\partial \mathcal{F}}{\partial x}\right)_i . \tag{57}$$

REFERENCES

1. A. G. Kravchenko and P. Moin, On the effect of numerical errors in large-eddy simulations of turbulent flows, *J. Comput. Phys.* **131**, 310 (1997).
2. A. Jameson, W. Schmidt, and E. Turkel, *Numerical Solutions of the Euler Equations by Finite Volume Methods Using Runge–Kutta Time Stepping*, AIAA Paper 81-1259, 1981.
3. C.-W. Shu, *Essentially Non-oscillatory and Weighted Essentially Non-oscillatory Schemes for Hyperbolic Conservation Laws*, ICASE Report No. 97-65, 1997.
4. M. Shur, P. R. Spalart, M. Strelets, and A. Travin, Detached-eddy simulation of an airfoil at high angle of attack, in *Int. Symp. Eng. Turb. Modelling and Measurements, Corsica, May 24–26, 1999*.
5. H. J. Kaltenbach and H. Choi, *Large-Eddy Simulation of Flow around an Airfoil on a Structured Mesh*, Center for Turbulence Research. Annual Research Briefs, Standford University, 1995.
6. F. Ducros, V. Ferrand, F. Nicoud, C. Weber, D. Darracq, and C. Gacherieu, Large-eddy simulation of shock-turbulence interaction, *J. Comput. Phys.* **152**, 517 (1999).
7. D. K. Lilly, On the computational stability of numerical solutions of time-dependent non-linear geophysical fluid dynamics problems, *Monthly Weather Rev.* **93**(1), 11 (1965).
8. Y. Morinishi, *Conservative Properties of Finite Difference Schemes for Incompressible Flow*, Center for Turbulence Research, Annual Research Briefs, 1995.
9. A. Arakawa, Computational design for long term numerical integrations of the equations of atmospheric motion, *J. Comput. Phys.* **1**, 119 (1966).
10. W. C. Reynolds, W. J. Feiereisen, and J. H. Ferziger, *Numerical Simulation of a Compressible Homogeneous Turbulent Shear Flow*, Rep. TF-13, Thermosci, Div., Department of Mech. Eng., Stanford University, 1981.
11. P. Lax and B. Wendroff, Systems of conservation laws, *Comm. Pure Appl. Math.* **13**, 217 (1960).
12. Y. Morinishi, T. S. Lund, O. Vasilyev, and P. Moin, Fully conservative high order finite difference schemes for incompressible flow, *J. Comput. Phys.* **143**, 90 (1998).
13. A. E. P. Veldman and R. W. C. P. Verstappen, Symmetry-conserving discretization with application to the simulation of turbulent flow, in *Numerical Methods for Fluid Dynamics, VI*, edited by M. J. Baines (ICFD Conference, 1998), p. 539.
14. R. W. C. P. Verstappen and A. E. P. Veldman, A comparison of low-order dns, high-order dns and les, in *2nd Ercoftac Workshop on Direct and Large-Eddy Simulation, 1998*.
15. G. A. Blaisdell, N. N. Mansour, and W. C. Reynolds, Compressibility effects on the growth and structure of homogeneous turbulent shear flow, *J. Fluid Mech.* **256**, 443 (1993).
16. K. S. Lele, Compact finite difference schemes with spectral-like resolution, *J. Comput. Phys.* **103**, 16 (1992).
17. A. Stoessel, A parallel tool for the study of 3d turbulent combustion phenomena, in *Proceedings of the Parallel CFD'95 Conference, Pasadena, 1995*.
18. C. Weber, F. Ducros, and A. Corjon, *Large-Eddy Simulation of Complex Turbulent Flows*, AIAA Paper 98-2651, 1998.
19. F. Ducros, C. Soulères, F. Laporte, P. Moinat, C. Weber, and V. Guinot, High-order skew-symmetric jameson schemes for unsteady compressible flows, in *Proceeding of the Ercoftac/Issac Newton Join Workshop, 1999*.
20. A. Jameson, Analysis and design of numerical schemes for gas dynamics. 1. Artificial diffusion, upwind biased, limiters and their effect on accuracy and multgrid convergence, *Comput. Fluid Dynam.* **4**, 171 (1995).
21. A. Jameson, Analysis and design of numerical schemes for gas dynamics. 2. Artificial diffusion and discrete schock structure, *Comput. Fluid Dynam.* **5**, 1 (1995).
22. R. C. Swanson and E. Turkel, On central-difference and upwind schemes, *J. Comput. Phys.* **101**, 292 (1992).
23. A. E. P. Veldman and K. Rinzema, Playing with nonuniform grids, *J. Eng. Math.* **26**, 119 (1992).

24. C. A. J. Fletcher, *Computational Techniques for Fluid Dynamics, Scientific Computation* (Springer-Verlag, New York, 1988), Vol. 2.
25. W. Colella and P. R. Woodward, The piecewise parabolic method (ppm) for gas-dynamical simulations, *J. Comput. Phys.* **54**, 174 (1984).
26. J. Vos, E. Chaput, B. Arlinger, A. Rizzi, and A. Corjon, Recent advances in aerodynamics inside the nsmb (navier–stokes multi-block) consortium, in *36th Aerospace Sciences Meeting and Exhibit, Reno, NV, January 12–15, 1998*, AIAA-98-0802.
27. C. Hirsh, *Numerical Computation of Internal and External Flow* (Wiley, New York, 1988), Vol. 1.
28. C. Weber, *Développement de méthodes implicites pour les équations de navier–stokes moyennées et la simulation des grandes échelles: Application à l'aérodynamique externe*, Thèse de l'INPT, Toulouse, France, 1998.
29. R. Hixon, *Evaluation of a High-Accuracy Maccormack-Type sche Using Benchmarck Problems*, NASA Contractor Report 202324, 1997.
30. G. A. Sod, A survey of several finite-difference methods for systems on non linear hyperbolic conservation laws, *J. Comput. Phys.* **27**, 1 (1978).
31. A. Bayliss, P. Parikh, L. Maestrello, and E. Turkel, *A Fourth-Order Scheme for the Unsteady Compressible Navier–Stokes Equations*, AIAA Paper 85 1694, 1985.
32. X. Normand and M. Lesieur, Direct and large eddy simulation of transition in the compressible boundary layer, *Theoret. Comput. Fluid Dynam.* **3** (1992).
33. H. Schlichting, *Boundary Layer Theory* (McGraw–Hill, New York, 1979).
34. L. M. Mack, *Boundary-Layer Stability Theory*, Rep. 900-277, Jet Propulsion Lab, Pasadena., 1969.
35. S. C. Crow, Stability theory for a pair of trailing vortices, *AIAA J.* **8**, 2172 (1970).
36. D. Bliss, S. E. Widnall, and A. Zalay, Theoretical and experimental study of the stability of a vortex pair, in *Aircraft Wake Turbulence and Its Detection*, edited by J. H. Olsen, *et al.* (Plenum, New York, 1971), p. 305.
37. P. Spalart and S. R. Allmaras, *A One-Equation Turbulence Model for Aerodynamic Flows*, AIAA Paper 92-0439, 1992.